Science of the Total Environment 792 (2021) 148426

Contents lists available at ScienceDirect

Science of the Total Environment

journal homepage: www.elsevier.com/locate/scitotenv

Elemental fingerprints in natural nanomaterials determined using SP-ICP-TOF-MS and clustering analysis

Mohammed Baalousha [a,*], Jingjing Wang [a], Mahdi Erfani [b], Erfan Goharian [b]

[a] Center for Environmental Nanoscience and Risk, Department of Environmental Health Sciences, Arnold School of Public Health, University of South Carolina, SC 29208, USA
[b] Department of Civil and Environmental Engineering, College of Engineering and Computing, University of South Carolina, SC 29208, USA

HIGHLIGHTS

- Natural nanomaterials (NNMs) were characterized using SP-ICP-TOF-MS.
- Baseline understanding of elemental purity and association in NNM was established.
- The elemental composition of the most dominant classes of NNMs was determined.

GRAPHICAL ABSTRACT

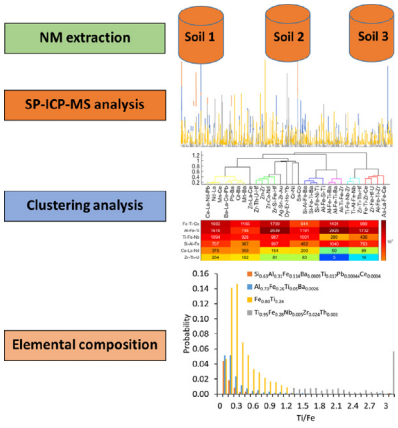

ARTICLE INFO

Article history:
Received 27 April 2021
Received in revised form 8 June 2021
Accepted 9 June 2021
Available online 15 June 2021

Editor: Damia Barcelo

Keywords:
Single particle-inductively coupled plasma-time of flight-mass spectrometer
Natural nanomaterials
Elemental composition and associations
Clustering analysis

ABSTRACT

Detection and quantification of engineered nanomaterials in environmental systems require precise knowledge of the elemental composition, association, and ratios in homologous natural nanomaterials (NNMs). Here, we characterized soil NNMs at the single particle level using single particle-inductively coupled plasma-time of flight-mass spectrometer (SP-ICP-TOF-MS) in order to identify the elemental purity, composition, associations, and ratios within NNMs. Elements naturally present as a major constituent in NNMs such as Ti, and Fe occurred predominantly as pure/single metals, whereas elements naturally present at trace levels in NNMs occurred predominantly as impure/multi-metal NNMs such as V, Nb, Pr, Nd, Sm, Eu, Gd, Tb, Er, Dy, Yb, Lu, Hf, Ta, Pb, Th, and U. Other elements occurred as a mixture of single metal and multi-metal NNMs such as Al, Si, Cr, Mn, Ni, Cu, Zn, Ba, La, Ce, W, and Bi. Thus, elemental purity can be used to differentiate ENMs *vs.* NNMs only for those elements that occur at trace level in NNMs. We also classified multi-metal NNM into clusters of similar elemental composition and determined their mean elemental composition. Six major clusters accounted for more than 95% of the detected multi-metal NNMs including Al-, Fe-, Ti-, Si-, Ce-, and Zr-rich particles' clusters. The elemental composition of these multi-metal NNM clusters is consistent with naturally occurring minerals. Titanium occurred as a major element (>70% of the total metal mass in NNMs) in Ti-rich cluster and as a minor (<25% of the total metal mass in NNMs) element in likely clay, titanomagnetite, and aluminum oxide phases. Two rare earth element (REE) clusters were identified, characteristic of light REEs and heavy REEs. The findings of this study provide a methodology and baseline information on the elemental composition, associations, and ratios of NNMs, which can be used to differentiate NNMs *vs.* ENMs in environmental systems.

* Corresponding author.
E-mail addresses: mbaalous@mailbox.sc.edu (M. Baalousha), jingwang@mailbox.sc.edu (J. Wang), merfani@email.sc.edu (M. Erfani), goharian@cec.sc.edu (E. Goharian).

https://doi.org/10.1016/j.scitotenv.2021.148426
0048-9697/

1. Introduction

As the production and use of engineered nanomaterials (ENMs) such as TiO_2, CeO_2, and La_2O_3 increases (Piccinno et al., 2012), so does the potential for their release to environmental systems (Lead et al., 2018). For instance, several studies demonstrated the release of high concentrations of TiO_2 engineered particles (*e.g.*, ENMs and pigments) from construction and demolition landfills (Kaegi et al., 2017), paints (Kaegi et al., 2008), bathing (Gondikas et al., 2014), sewage spills (Loosli et al., 2019a), and urban runoff (Wang et al., 2020; Durin, 2006). Thus, there is an increased need to develop analytical approaches to quantify the concentrations and characterize the properties of ENMs in complex environmental matrices including soils and sediments (Alvarez et al., 2009). However, these environmental matrices encompass high concentrations of naturally occurring nanomaterials (NNMs) with similar elemental compositions and particle size as ENMs, which complicates the detection and quantification of ENMs in such systems (Praetorius et al., 2017; Philippe et al., 2018). For instance, Ti- and Ce-rich particles are naturally present in soils and sediments at much higher concentrations than the estimated ENM environmental concentrations (Gottschalk et al., 2013). The detection and quantification of ENMs in environmental matrices require differentiating ENMs from NNMs (von der Kammer et al., 2012; Montano et al., 2014). Therefore, a precise knowledge of the properties of NNMs such as size distribution, elemental composition, and elemental ratios is a prerequisite to develop strategies for the detection and quantification of ENMs in the natural environment.

In soils, natural particles form after weathering of parent material and generally exhibit similar elemental compositions, associations, and ratios as those of the parent rocks. Some elements are almost exclusive to only one or two minerals such as Zr and Hf, which are only associated with zircon. The elements Nb, Ti, and Ta often have similar mineralogical affinities, being associated with titanium minerals such as rutile, anatase, sphene, and/or opaque heavy minerals (*e.g.*, titanomagnetite, magnetite, and ilmenite) (Craigie, 2018). Natural TiO_2 minerals, such as rutile and ilmenite, have been shown to be the dominant carrier (*e.g.*, >90–95% of the whole rock content) for Ti, Nb, Ta, Sb, and W as well as an important carrier (*e.g.*, 5–45% of the whole rock content) for V, Cr, Mo, and Sn in TiO_2-bearing metamorphic rocks (Zack et al., 2002; Gaspar and Wyllie, 1983). The elements Th, Y, and heavy rare earth elements (HREEs) are concentrated exclusively in heavy minerals (Craigie, 2018). Cerium is the most abundant REE and is typically associated with other rare earth elements such as La, Er, Eu, Ho, Tm, Y, Yb in minerals such as monazite, xenotime, allanite, bastnasite, and others (Murata et al., 1957; Long et al., 2012).

Elemental impurities are generally removed during the manufacturing of ENMs (*e.g.*, TiO_2 and CeO_2) from natural parent minerals resulting in pure ENMs (International Agency for Research on Cancer, 2010; Baalousha et al., 2020). Thus, a promising approach to differentiate natural from engineered particles is based on detecting elemental impurities and determining elemental ratios in NNMs (Loosli et al., 2019a; Gondikas et al., 2018). Elemental ratios such as Ti/Nb, Ti/Ta, and Ti/Al of bulk waters and soils have been recently used to quantify TiO_2 engineered particles in sewage spills (Loosli et al., 2019a), urban runoff (Wang et al., 2020), and stormwater green infrastructures (Baalousha et al., 2020). Additionally, elemental ratios such as Zr/Nb, Zr/Th, Th/Nb, Ti/Ta, and Cr/Nb have been used in the identification of chemozones (Craigie, 2018). The benefits of using these elemental associations and ratios are that they are generally very 'stable' and largely unaffected by post-depositional diagenesis or weathering (Craigie, 2018). Nonetheless, these elemental associations and ratios could be altered by environmental processes such as dissolution due to changes in environmental conditions (*e.g.*, pH and redox potential), or during particle extraction (Regelink et al., 2013). Natural particle extraction from soil microaggregates is vital to simplify their characterization by reducing natural sample polydispersity and to improve the understanding of NNM physicochemical properties such as size distribution, elemental composition and ratios, and morphology (Loosli et al., 2019b; Yi et al., 2020; Loosli et al., 2019c). However, chemical extractants and extraction conditions (*e.g.*, tetrasodium pyrophosphate and high pH) could dissolve soluble particles such as iron oxides, which may impact the elemental ratios (*e.g.*, Ti/Fe) (Regelink et al., 2013).

Multi element-single article analysis by single particle-inductively coupled plasma-time of flight-mass spectrometer (SP-ICP-TOF-MS) is a promising technique in the nanometrology toolbox to differentiate ENMs from NNMs based on elemental purity/impurity and elemental ratios at the single particle level (Loosli et al., 2019a; Praetorius et al., 2017). The premise of ICP-TOF-MS is that it detects and quantifies all elements within a single particle at low/trace concentrations, and thus, ICP-TOF-MS is the only method that could be implemented to differentiate ENMs from NNMs in environmental systems at the single particle level. However, ICP-TOF-MS detects and quantifies elements that occur within particles at concentrations greater than the minimal detectable mass (MDM, Table S1), which is element dependent (Lee et al., 2014; Hadioui et al., 2019). The MDM that can be attained with SP-ICP-MS depends on the instrument or elemental sensitivity and the background levels that result from both dissolved analyte and instrumental noise (electronic noise and interferences to the monitored isotope) (Hadioui et al., 2019). Thus, the ability of the ICP-TOF-MS to "unequivocally" differentiate ENMs from NNMs based on elemental purity/impurity and elemental ratios at the single particle level remains uncertain.

This study aims to generate baseline information on elemental purity, associations, and composition of NNMs extracted from soil samples and investigate how these parameters are impacted by the extractant composition. NNMs were extracted from three topsoils by both ultrapure water and tetrasodium pyrophosphate and were characterized by SP-ICP-TOF-MS.

2. Materials and methods

2.1. Soil samples

Three topsoil samples were collected with a hand drill from the surface to 15 cm below the surface in polyethylene bags. The first topsoil (Orangeburg) was collected from Dillon County (34.5044, −79.4231452), South Carolina, United States. The soil is characterized as Orangeburg series. The Orangeburg series consists of very deep, well-drained, moderately permeable soils on the uplands of the Southern Coastal Plain. They are formed in loamy and clayey marine sediments. The topsoil is characterized as a dark grayish brown loamy sand with a weak fine granular structure. The second topsoil (Varina) was from collected Dillon County (34.455574, −79.444813), South Carolina, United States. This soil is characterized as Varina series formed from sandy loam. The topsoil is characterized as grayish brown sandy loam with a weak fine granular structure. The third topsoil (Mecklenburg) was collected from Chester County (34.80189, −80.07951139), South Carolina, United States. This soil is characterized as Mecklenburg series. The Mecklenburg series consists of very deep, well-drained, slowly permeable soils that formed in residuum weathering from intermediate and mafic crystalline rocks of the Piedmont uplands. The topsoil was characterized as a reddish-brown loam with a moderate medium granular structure.

2.2. Natural particle extraction

The collected soils were sieved using a 10-mesh 2 mm pore size nylon sieve (Zhangxing Instrument, Hangzhou, Zhejiang, China) to remove large particles. A hundred grams of the dry-sieved soils were mixed with 1 L UPW for 24 h, followed by wet sieve through a 300-mesh 54 μm pore size nylon sieve (Zhangxing Instrument, Hangzhou, Zhejiang, China). Then, the sieved soil samples were transferred into

Fast-Freeze flasks for freeze-drying (Freezone 6, Labconco, Kansas City, MO, USA) to achieve complete dryness. The dried samples were stored in 50 mL acid-washed polypropylene centrifuge tubes (Fisherbrand, Fisher Scientific, San Nicolás de Los Garza, Mexico) in a freezer before further treatment.

Two solutions were used to extract NMs from soils: 1) ultrapure water (UPW) as a minimally disturbing extractant and 2) tetrasodium pyrophosphate solution at pH 10 as it has been shown to improve NM extraction from soils and waters (Loosli et al., 2019b; Yi et al., 2020; Loosli et al., 2019c; Loosli et al., 2018). Twenty mg of the freeze-dried soils were mixed with 30 mL UPW (PURELAB Option-Q, ELGA, Buckinghamshire, UK) or 10 mM tetrasodium pyrophosphate solution at pH 10 (analytical grade, Alfa Aesar, Japan) in 50 mL acid-washed polypropylene centrifuge tubes and overhead rotated on a tube rotator (Fisher Scientific, Shanghai, China) at 40 rpm overnight. The well-dispersed mixture was bath sonicated (Branson 2800, 40 kHz, Eppendorf, Hamburg, Germany) for 2 h to disrupt soil microaggregates and enhance the release dispersion of natural particles (Loosli et al., 2018). The 1 μm size fraction was then separated by centrifugation (Eppendorf, 5810 R, Germany) at 775 g for 5 min based on a particle density of 2.5 $g \cdot cm^{-3}$ and Stokes' law calculation (Tang et al., 2009). The top 20 mL of the supernatant was transferred into 50 mL acid-washed polypropylene centrifuge tubes and stored at 4 °C before any further analysis. The collected fractions were diluted 5000-folds in UPW and sonicated for 15 min in a bath sonicator prior to SP-ICP-TOF-MS analysis.

2.3. Single particle analysis

Single particle analysis of the diluted soil NNM extracts was performed using an ICP-TOF-MS (TOFWERK, Thun, Switzerland) to determine all isotopes within a single particle simultaneously (Hendriks et al., 2017). All samples and UPW blanks were analyzed in triplicates and data were collected for 200 s for each replicate. The replicates were combined for all following data analysis due to the low detection frequency of some elements. Element specific instrument sensitivities were measured with a series of multi-element solutions prepared from a mixed multi-element ICP certified reference standard (0, 1, 2, 5, and 10 μg L^{-1} multi-element standard, diluted in 1% HNO_3, BDH Chemicals, Radnor, PA, USA). The transport efficiency was calculated using the known size approach (Pace et al., 2011) using both Au ENMs with a certified particle size of 60 nm (NIST RM8013 Au, Gaithersburg, MD, USA) prepared in UPW and Au ionic standard solutions (0, 1, 2, 5, and 10 μg L^{-1}, diluted in 1% HCl, BDH Chemicals, West Chester, PA, USA). Using a standard tuning solution, the ICP-TOF-MS mass spectra were calibrated based on $^{18}H_2O^+$, $^{59}Co^+$, $^{115}In^+$, $^{140}Ce^+$, and $^{238}U^+$ target isotopes in TofDaq Viewer (Version, TOFWERK) prior analysis or in Tofware (Version, TOFWERK) after analysis if mass shifts occurred during analysis. Particle/baseline signal separation, particle signals, particle mass, and particle number concentration were determined from the mass-calibrated ICP-TOF-MS spectra using Python script in Tofware as described elsewhere (Loosli et al., 2019a). The particle detection threshold was calculated for each isotope according to Eq. (1) (Tanner, 2010).

$$\text{Threshold} = \text{Mean} + (3.29\sigma + 2.71) \quad (1)$$

Mean and σ are those of background signal in the analysis window of 100 data points. The data for each isotope were treated separately, but the time stamps were kept throughout the data processing for every isotope, allowing for the identification of isotope correlations in a single particle. For example, an impure particle (*e.g.*, a particle containing multiple elements) generates several isotope signals spikes in a given time stamp. An "apparently pure" particle generates one isotope signal spike in a given time stamp. The term "apparently pure" is used in this study because such particles might contain elements at a concentration below the sp-ICP-MS minimum detectable mass (MDM, Table S1). All results are discussed below in term of the number of detected particles under the experimental conditions (*e.g.*, transport efficiency = 6%, sample flow rate = 0.4 mL min^{-1}, combined triplicate analysis of 200 s each, and dilution factor = 5000 folds were constant for all samples). These parameters can be used to calculate the actual number concentration of NNMs in the soils as described elsewhere (Pace et al., 2011).

2.4. Automated clustering to discover metallic fingerprint in NNMs

Clustering analysis was performed, using MATLAB, to identify clusters/groups of NNMs of similar elemental composition and to identify their mean elemental composition, with the aim to identify unique metallic fingerprints in NNMs. Multi-metal containing NNMs were processed through a two-stage (*e.g.*, intra- and inter-sample) K-median hierarchical clustering analysis following the method described elsewhere (Mehrabi et al., 2021). First, intra-sample clustering was performed on all metal masses in each NNM to generate clusters that best account for variance in NNM metallic composition in each sample. Correlation distance, which represents the dissimilarity of NNM composition to one another, was used as the distance metric for clustering. A lower correlation distance indicates that the elemental compositions of two particles are very close to each other and *vice versa*. This step generates a cluster dendrogram for each sample, which was divided into major clusters using a distance cutoff. The distance cutoff was determined by visually inspecting the dendrogram and through trial and error in order to minimize the variance/diversity in NNM elemental composition in the major clusters. A cluster representative was determined for each major cluster as the median of metal mass in individual NNMs within each cluster. For each major cluster, the mass fraction of a given metal in each particle was determined as the mass of that metal divided by the sum of masses of all metals in that particle. Then, the mean cluster composition was determined as the mean of metal mass fraction in all particles in the cluster. Similarly, the elemental ratios were determined on a particle-per-particle basis and the mean and standard deviation of elemental ratios were determined by taking into account all particles that contain the two metals for which elemental ratios were calculated. Second, inter-sample clustering was performed on the major cluster representatives identified in the intra-sample clustering to group/cluster the similar NNM major clusters identified in the different samples. This step generates a cluster dendrogram for intra-sample cluster representatives, which was divided into major clusters using a distance cutoff as performed for the intra-sample clusters. Finally, heat maps were generated by comparing the number of NNMs in similar major clusters among the different samples.

3. Results and discussion

3.1. Elemental associations in single particles

The total number of detected, single metal (apparently pure), and multi-metal (impure) NNMs are presented in Fig. 1. Few metals, Si and Fe more frequently, were detected as single particles in the blanks (Fig. 1a). Most of the detected metals in the blanks were single metal particles (Fig. 1b and d). Contrary, multi-metal containing particles were rarely detected in the blanks suggesting that all multi-metal containing particles are true NNMs (Fig. 1c, and e).

Elements such as Ti, Fe, Zn, Sb, and Sn occurred dominantly as single metal NNMs (Fig. 1d). This is likely because natural impurities are present in Ti, Fe, Zn, Sb, and Sn-rich minerals/particles at low concentrations, potentially below the SP-ICP-MS MDM. Other metals such as V, Nb, Pr, Nd, Sm, Eu, Gd, Tb, Dy, Ho, Er, Yb, Lu, Hf, Ta, Pb, Th, and U occurred predominantly as multi-metal NNMs (Fig. 1e). This is most likely because these metals occur as minor constituents in other mineral phases such as Fe-, Ti-, Ce-, and Zr-containing particles. Other elements such as Al, Si, Cr, Mn, Ni, Cu, Zr, Ba, La, Ce, W, and Bi occurred as a mixture of single metal and multi-metal containing particles. These

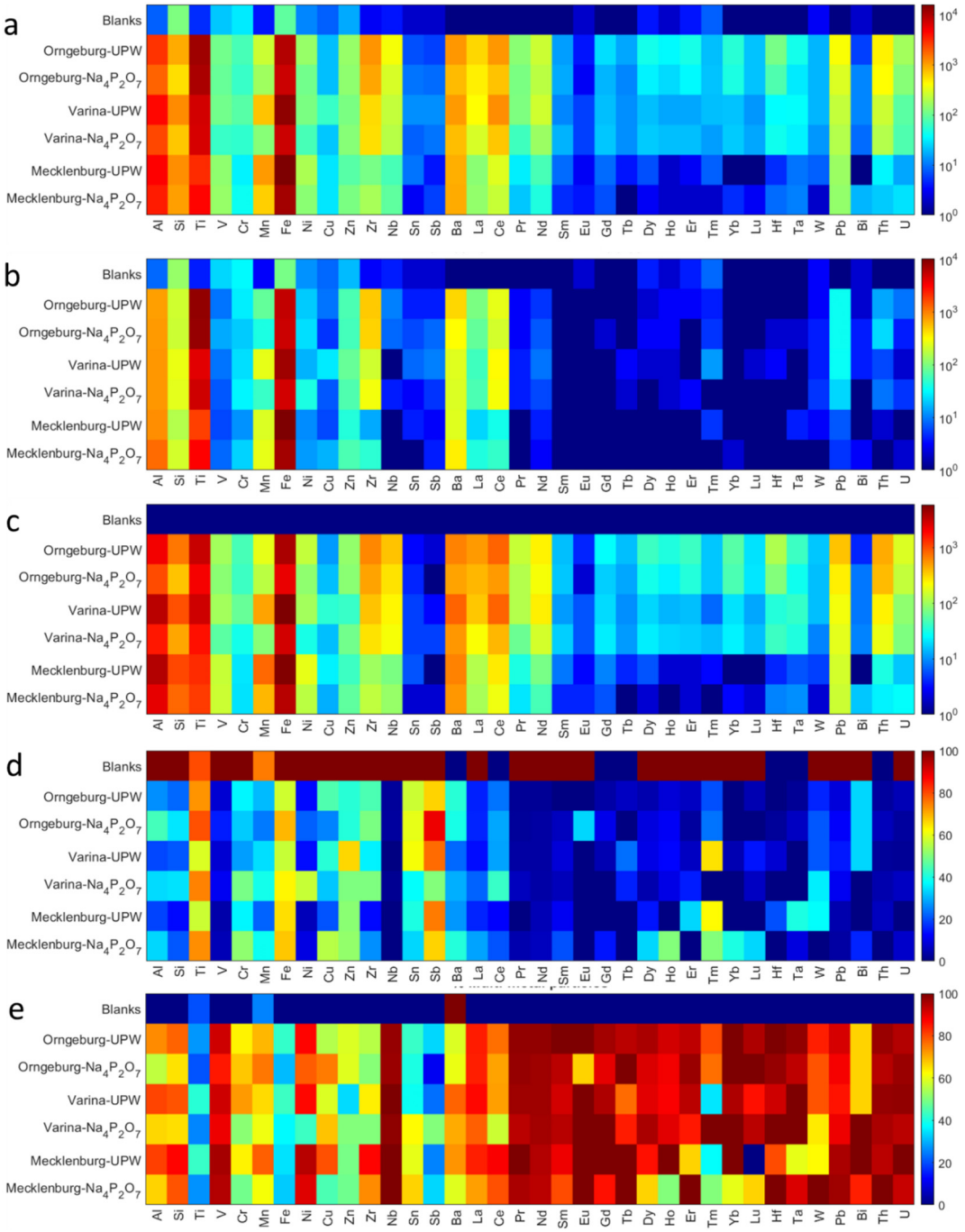

Fig. 1. Heat maps illustrating the number of (a) detected, (b) single metal (apparently pure), (c) multi-metal (impure), (d) % of single metal, and (e) % of multi-metal natural nanomaterials in three soils in South Carolina. Natural nanomaterials were extracted using ultrapure water (UPW) and sodium pyrophosphate ($Na_4P_2O_7$).

elemental associations indicate the possibility to differentiate NNM *vs.* ENMs based on particle purity/impurity is limited only to those few metals that occur predominantly as impure NNMs.

In general, a higher number of total, single metal, and multi-metal particles were detected for most elements in UPW-extracted suspensions than in $Na_4P_2O_7$-extracted suspensions (Fig. 1a, b, and c). This is likely due to the increased disaggregation of natural heteroaggregates in $Na_4P_2O_7$-extracted suspensions (Baalousha et al., 2020; Yi et al., 2020), resulting in the release of small particles (small masses) that are lower than the SP-ICP-TOF-MS MDM. This observation is supported by the increase in the Ti and Fe background levels and the dissolved concentrations, measured by SP-ICP-MS, in $Na_4P_2O_7$-extracted suspensions compared with those in UPW extracted suspension (Figs. S1c, 2c and 3).

The discussion below focuses on elemental associations in some of the most detected multi-metal NNMs including Ti-, Zr-, and Ce-rich NNMs.

Multi-metal Ti-containing particles contained at least one natural impurity such as Fe, Al, Si, Zr, Nb, Th, Ce, Ba, Mn, Pb, Ni, Zn, La, V, U, Ta, Nd, Cr, Pr, Cu, and W (Fig. S4), indicating that these particles are most likely naturally occurring particles. This is in good agreement with the elemental association between Ti and other elements in natural surface waters in Lake Katherine in Columbia, South Carolina, United States (Loosli et al., 2019a). This is also in good agreement with the impurities (*e.g.*, Nb, Ta, Sb, W, V, Cr, Mo, and Sn, Zr, Fe, U and Pb) detected in natural TiO_2 minerals such as rutile and ilmenite) (Zack et al., 2002; Gaspar and Wyllie, 1983; Nakashima and Imaoka, 1998). The relative abundance of Ti particles containing some natural impurities (*e.g.*, Fe and Al) was

lower in the $Na_4P_2O_7$-extracted suspensions compared to those in UPW-extracted suspensions (Fig. S4a), which can be attributed to the increased disaggregation or dissolution of the natural impurities in $Na_4P_2O_7$-extracted suspensions as discussed above (Baalousha et al., 2020; Yi et al., 2020). Such processes can occur in natural environmental systems due to changes in water chemistry such as pH, redox potential, and natural organic matter, which may impact elemental associations and ratios in natural particles. However, the relative abundance of other natural impurities (*e.g.*, Nb and Pb) in Ti-containing particles did not change as a function of extractant (Fig. S4a). These results indicate a strong association between Ti and Nb, Ti and Pb, and a weaker association between Ti and Fe, and Al within Ti-containing NNMs. Only a few particles contained Nb, representing <5% of the total number of Ti-containing particles (Table S2). This is likely due to the low concentrations of Nb in Ti-containing particles, rendering Nb undetectable in most Ti-containing particles. The concentration of Nb in Ti-containing particles is 20 to 400 times lower than Ti concentration (Loosli et al., 2019a). Given the similar ionization efficiency of Ti and Nb in the ICP, Nb can be detected only in Ti particles with masses 20–400 times the mass of Nb-MDM by SP-ICP-TOF-MS.

Multi-metal Zr-containing particles contained natural impurities such as Al, Si, Ti, Fe, Mn, Nb, Ta, Th, U, Hf, Zn, Ni, Cr, Pb, Ba, La, Ce, Nd, Ho, Tm, Dy, Er, Yb, and Lu (Fig. S4b). These impurities are in good agreement with the impurities reported in ZrO_2 natural minerals (Fitzpatrick and Chittleborough, 2002). Zircon ($ZrSiO_4$) is the most abundant Zr mineral. Baddeleyite (ZrO_2) is the most common of the zirconium oxides, but many less common oxides such as calzirtite and zirconolite may also occur in soils (Fitzpatrick and Chittleborough, 2002). Hafnium is a common substituent in zircon, and Y and other REEs also occur at lower concentrations. Uranium, Th, and Pb are also important minor elements in zirconium oxides. Substituents for Si in tetrahedral sites include Al, and Fe can also be associated with Zr (Fitzpatrick and Chittleborough, 2002).

Multi-metal Ce-containing particles were associated with 33 other elements with La being the most detected element in Ce-containing particles (Fig. S4c). Multi-metal La-containing particles were associated with 18 other elements with Ce being the most detected in La-containing particles (Fig. S4d). These impurities are in good agreement with the impurities reported in Cerium oxide and Lanthanum oxide NNMs. For instance, the associations between Ce, La, Pr, and Nd, are consistent with the fact that REE containing minerals are usually dominated by either other light or heavy rare earth elements (LREEs or REES) (Haque et al., 2014). In addition to REE species, many minerals contain high levels of REEs substituting for other cations of comparable radius and charge. For instance, mosandrite [$(Ca, Na)_{3-x}(Ca, REE)_4TiSi_2O_7)_2(OH, F, H_2O)_4.H_2O$], apatite [$(Ca, REE, Sr, Na)_5(P,Si)_3O_{12}(F,OF,Cl)$], ewaldite [$Ba(Ca,Na,REE)(CO_3)_2 \cdot nH_2O$], and perovskite [$(Ca,Na,REE)(Ti, Nb,Fe)O_3$] commonly incorporate $1–2 \times 10^5$ ppm REE in the Ca site in their structure. Additionally, numerous other minerals may exhibit enrichment in REEs depending on their crystallization conditions; a few notable examples include titanite ($CaTiSiO_4O$), zircon ($ZrSiO_4$), eudialyte (Na—Ca—Mn—Fe—Zr cyclosilicate), pyrochlore [$Ca,Na)_{2-x}(NbTi)_2O_6(F,OH)$], and members of the carnallite group [$(Ca,Sr,Ba,Pb)(Al,Fe)_3(PO_4)_2(OH)_5$] (Chakhmouradian and Wall, 2012).

Almost all Nb-containing NNMs (*e.g.*, 95 to 100%, Table S3) were associated with Ti-containing particles. Similarly, almost all Hf-containing particles (*e.g.*, 90 to 100%, Table S4) were associated with Zr-containing particles. This is because Nb and Hf occur almost exclusively in Ti and Zr minerals at lower concentrations than Ti and Zr, respectively (Craigie, 2018). Zr and Hf are only associated with zircon. Nb, Ti, and Ta are associated with titanium minerals such as rutile, anatase, sphene, and/or opaque heavy minerals (*e.g.*, titanomagnetite, magnetite, and ilmenite) (Montano et al., 2014). Natural TiO_2 minerals (*e.g.*, rutile and ilmenite) are the dominant carriers (>90–95% of whole rock content) for Nb, Ta, Sb, and W (Gaspar and Wyllie, 1983; Nakashima and Imaoka, 1998). Ti and Zr are always detectable in Nb- and Hf-containing particles because Ti and Zr occur always at higher concentrations than Nb and Hf in natural minerals and because Ti, Nb, Zr, and Hf are ionized efficiently (>92%) in the ICP (Chakhmouradian and Wall, 2012). Therefore, association with Ti and Zr is sufficient to differentiate natural from anthropogenic Nb-containing and Hf-containing particles, respectively, on a single particle basis. Additionally, the strong association of Nb with Ti and Hf with Zr, suggests that Nb and Hf are good tracers for Ti and Zr concentration based on total elemental ratios, but not at the single particle level as they only account for <5% of Ti- and Zr-containing particles detected by SP-ICP-TOF-MS.

3.2. Elemental ratios in single particles

The elemental ratios of Ti/Fe, Ti/Al, Ti/Nb, and Ce/La were calculated in single particles (Fig. 2) and the mean values are provided in Table 1. For the same soil, the mean elemental ratio of Ti/Fe was higher in the $Na_4P_2O_7$-extracted suspensions than those in the UPW-extracted suspensions (Table 1). This is likely due to the dissolution of iron oxides in the presence of pyrophosphate at high pH (*e.g.*, pH of 10) as observed elsewhere (Regelink et al., 2013). The elemental ratio distributions of Ti/Fe follow the same trend in the three soils (Fig. 2a and b), with the majority (*e.g.*, 67 to 89%) of particles displaying Ti/Fe in the range of 0 to 2.0, and a small fraction (*e.g.*, 10 to 28%, Table S5) exhibiting Ti/Fe > 2.0. Ti and Fe occur in natural minerals such as: titanomagnetite ($Fe_{3-x}Ti_xO_4$, $0 < Ti/Fe < 0.43$, $0 < x < 1$) which form a complete solid solution series between end members of magnetite (Fe_3O_4, Ti/Fe = 0); ulvöspinel (Fe_2TiO_4, Ti/Fe = 0.43); pseudobrookite (Fe_2TiO_5, Ti/Fe = 0.43); ilmenite ($FeTiO_3$, Ti/Fe = 0.86); pseudorutile ($Fe_2Ti_3O_9$, Ti/Fe = 1.29); and ilmenorutile and ferropseudobrookite ($FeTi_2O_5$, Ti/Fe = 1.71) (Fig. 2a). The higher Ti/Fe elemental ratios (*e.g.*, Ti/Fe = 2 to 20) can be attributed to either the aggregation of natural Ti-particles containing Fe and natural Ti-particles that do not contain Fe, or due to the presence of Fe-depleted naturally occurring Ti-particles. Fe—Ti oxides might be subject to alteration or weathering resulting in higher Ti/Fe elemental ratios (Weibel, 2003). For instance, the alteration of ilmenite occurs through several intermediate phases, each is successively enriched in titanium and depleted in iron (increasing Ti/Fe ratio), to an almost pure form of TiO_2 (Weibel, 2003; Mücke and Chaudhuri, 1991; Morad and Adin Aldahan, 1986; Morad, 1986). The alteration of ilmenite results in the formation of pseudorutile, fine leucoxene, and coarse leucoxene (leucoxene is a polycrystalline aggregate of rutile) (Weibel, 2003). Differences in Ti/Fe ratios between soils may indicate the degree of weathering of the ilmenite (Fitzpatrick and Chittleborough, 2002).

For the same soil, the mean elemental ratio of Ti/Al calculated was slightly higher in the $Na_4P_2O_7$-extracted suspensions and the UPW-extracted suspensions (Table 1). The Ti/Al distributions follow the same trend in the three soils (Fig. 2c and d), with the majority (*e.g.*, 88 to 93%) of particles displaying Ti/Al in the range of 0 to 0.4, and a small fraction (*e.g.*, 6.6 to 12.5%, Table S6) exhibiting Ti/Al > 0.4. These Ti/Al elemental ratios are in good agreement with those in natural minerals such as: palygorskite and montmorillonite (Ti/Al = 0.014–0.016); illite (Ti/Al = 0.026); kaolinite and hectorite (Ti/Al = 0.06); vermiculite and corrensite (Ti/Al = 0.090–0.093) (Fig. 2c). The slightly higher % of NNMs with Ti/Al > 0.4 in the $Na_4P_2O_7$-extracted suspensions than those in the UPW-extracted suspensions (Table S6) might be attributed to the increased disaggregation of natural heteroaggregates in the presence of $Na_4P_2O_7$ (Baalousha et al., 2020; Yi et al., 2020).

For the same soil, the mean elemental ratio of Ti/Nb was generally similar in the $Na_4P_2O_7$-extracted suspensions and the UPW-extracted suspensions (Table 1). The Ti/Nb distributions follow the same trend in the three soils (Fig. 2e and f), with the majority (*e.g.*, 83 to 96%) of particles displaying Ti/Nb in the range of 0 to 400, and a small fraction (*e.g.*, 4.8 to 17%, Table S7) exhibiting Ti/Nb > 400. The similarity in the Ti/Nb ratios for the UPW- and the $Na_4P_2O_7$-extracted suspensions is likely due to the lack of dissolution of Nb or disaggregation of Ti- and Nb-containing particles under the current experimental conditions. The

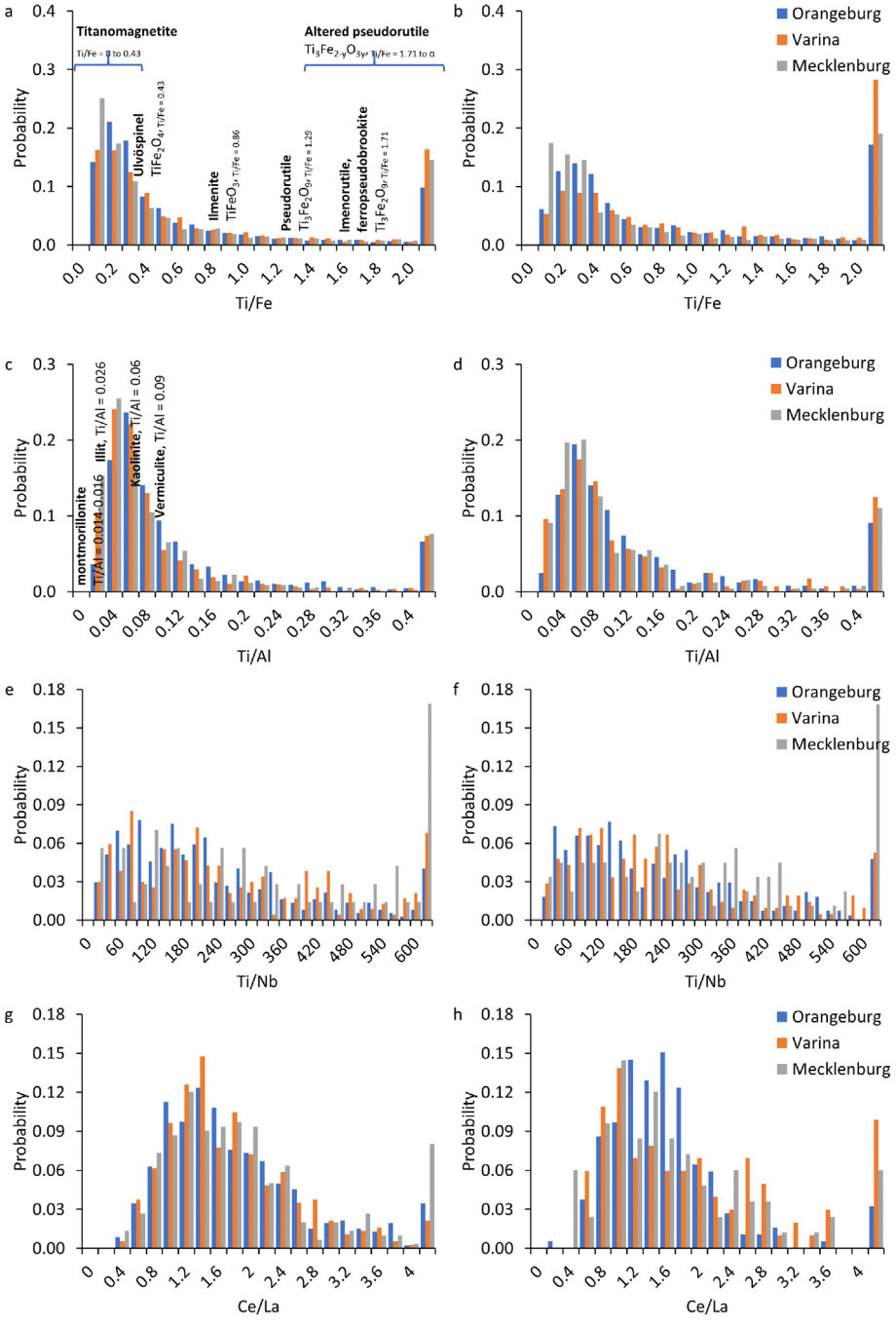

Fig. 2. Elemental ratios at the single particle level in (a, c, e, and g) ultrapure water (UPW)-extracted natural nanomaterial suspensions, and (b, d, f, and h) $Na_4P_2O_7$-extracted nanomaterial suspensions: (a and b) Ti/Fe, (c and d) Ti/Al, (e and f) Ti/Nb, and (g, h) Ce/La in three soils in South Carolina.

Table 1
Elemental ratios calculated on a single particle basis. Elemental ratios are reported as mean ± standard deviations (distribution) of the ratios calculated at the single particle level within a given sample.

	UPW			$Na_4P_2O_7$		
	Orangeburg	Varina	Mecklenburg	Orangeburg	Varina	Mecklenburg
Ti/Fe	0.82 ± 1.6	1.22 ± 2.3	1.11 ± 4.71	1.36 ± 2.3	2.09 ± 3.40	1.23 ± 2.60
Ti/Al	0.15 ± 0.37	0.22 ± 0.85	0.34 ± 1.54	0.24 ± 0.75	0.41 ± 1.44	0.29 ± 0.97
Ti/Nb	218 ± 176	268 ± 240	356 ± 309	223 ± 185	237 ± 200	355 ± 328
Ce/La	1.75 ± 0.99	1.89 ± 1.48	2.09 ± 2.20	1.74 ± 1.28	1.60 ± 1.22	1.85 ± 1.92
Zr/Hf	35.2 ± 31.1	43.4 ± 26.0	–	33.8 ± 22.3	41.6 ± 22.3	28.7 ± 16.6

variability in the Ti/Nb among the different soils might be due to 1) natural variability in Ti and Nb concentrations in the different soils, or 2) the small number of counted particles due to the low Nb content in Ti containing particles. These results further illustrate the strong association between Nb and Ti in NNM.

The mean elemental ratio of Ce/La on a single particle basis was consistent for the three soils and was slightly higher (*e.g.*, 1.75 ± 0.99 to 2.09 ± 2.20) for UPW-extracted suspensions compared to the corresponding elemental ratio (*e.g.*, 1.60 ± 1.22 to 1.85 ± 1.92) for $Na_4P_2O_7$-extracted suspensions (Table 1), which might be due to the disaggregation and/or dissolution of Ce- and La-containing minerals. The Ce/La distributions follow the same trend in the three soils and are centered at 1.4 and spans the range between 0.4 and 4 (Fig. 2g and h). These Ce/La ratios are consistent with those of the average crustal value, the average riverine particle ratio (2.1 and 2.0, respectively, Table S7), and in naturally occurring REE minerals such as monazite, xenotime, allanite, bastnasite, and others (Murata et al., 1957; Long et al., 2012).

3.3. Identification and composition of multi-metal particle clusters

For a better understanding of the elemental composition of natural NNM, multi-metal NNMs were clustered using a two-step hierarchical clustering. Ten to fourteen multi-metal NNM major clusters were identified in each soil NNM suspension (Fig. S5). These clusters include Al, Fe, Ti, Si, Ce, Dy, Zr, Mn, Cr, Pb, Cu, and Zn-containing particles. The top six clusters were Al, Fe, Ti, Si, Ce, and Ze-rich particle clusters and accounted for the large majority of multi-metal NNMs (>95% of the detected multi-metal NNMs) in all soil samples (Fig. 3). The mean mass fraction of each element in these clusters illustrates that these clusters are typical of aluminum oxides with minor concentrations of Fe and Ti (Fig. 4a), iron oxides with minor concentrations of Ti (Fig. 4b), titanium oxides with minor concentrations of Fe and trace concentrations of Nb and Th (Fig. 4c), clays with minor concentrations of Fe and Ti (Fig. 4d), LREE minerals (Fig. 4e), zirconium oxides with minor concentrations of Th, U, Hf, Yb, Er, and Tm (Fig. 4f), and HREE minerals (Fig. 4g). No striking difference in the elemental composition of these clusters was observed between the three soil samples, nor as a function of extractant composition (Fig. 4). Nonetheless, a higher number of particles were detected in most clusters in UPW-extracted suspensions compared to $Na_4P_2O_7$-extracted suspensions (Fig. 3), which can be attributed to the increased disaggregation or dissolution of the natural heteroaggregates in $Na_4P_2O_7$-extracted suspensions (Baalousha et al., 2020; Yi et al., 2020), resulting in the release of smaller (lower mass) multi-metal NNMs, lower than the SP-ICP-TOF-MS MDM. The same NNM cluster compositions also were observed (data not presented here) in surface waters in South Carolina including the Congaree and the Edisto Rivers, representing urban and rural rivers.

Four major clusters accounted for most of Ti- and Fe-containing particles (*e.g.*, Al—Fe—Ti, Fe—Ti—Ce, Ti—Fe—Nb, and Si—Al—Fe clusters, Fig. 3). The distribution of Ti/Fe in the individual particles in each cluster is presented in Fig. 5, together with the mean cluster composition. The Ti/Fe ratios in these clusters are consistent with those ratios in naturally occurring Ti-containing particles such as clay particles (Si/Al mass ratio = 2.1), aluminum oxides (Corundum is a crystalline form of aluminum oxide (Al_2O_3) typically containing traces of iron, titanium, vanadium and chromium) (Anthony, 1990), titanomagnetite ($0 < Ti/Fe < 0.43$), ilmenite (Ti/Fe = 0.86), pseudorutile (Ti/Fe = 1.29), ilmenorutile and ferropseudobrookite (Ti/Fe = 1.71), and altered pseudorutile (Ti/Fe > 1.71) (Weibel, 2003; Mücke and Chaudhuri, 1991; Morad and Adin Aldahan, 1986; Morad, 1986). In the TiFeNb cluster, the proportion of particles with Ti/Fe > 3.0 was higher in

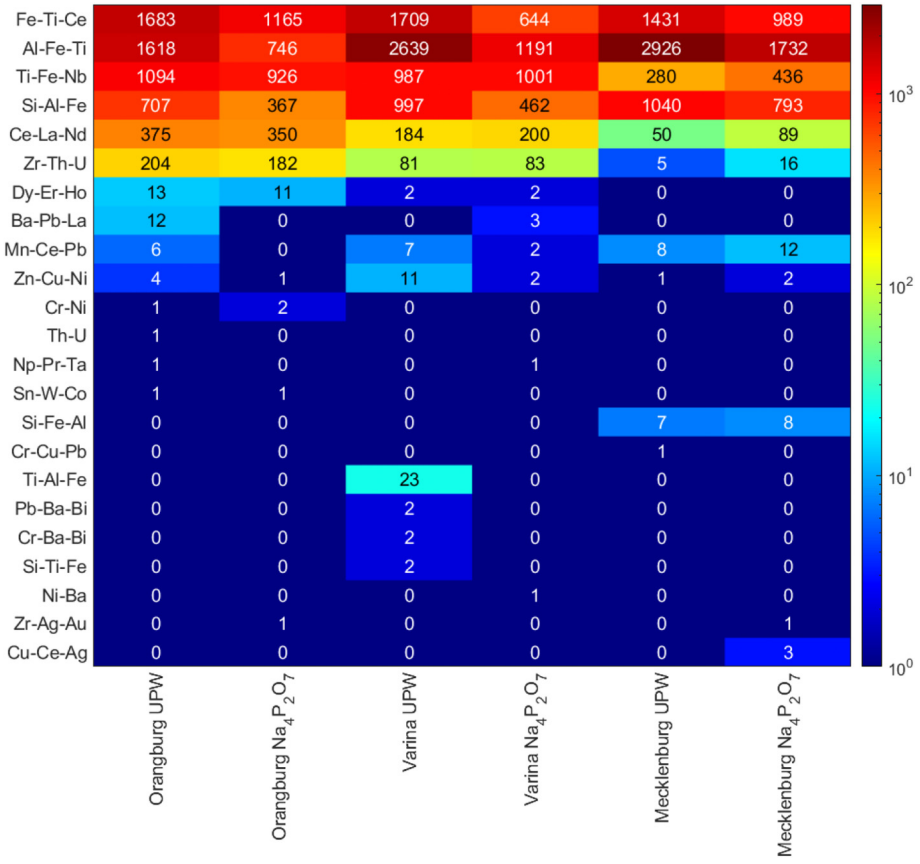

Fig. 3. Heat map of number of multi-metal nanomaterials in each cluster in three soils in South Carolina. Natural nanomaterials were extracted using ultrapure water (UPW) and sodium pyrophosphate ($Na_4P_2O_7$).

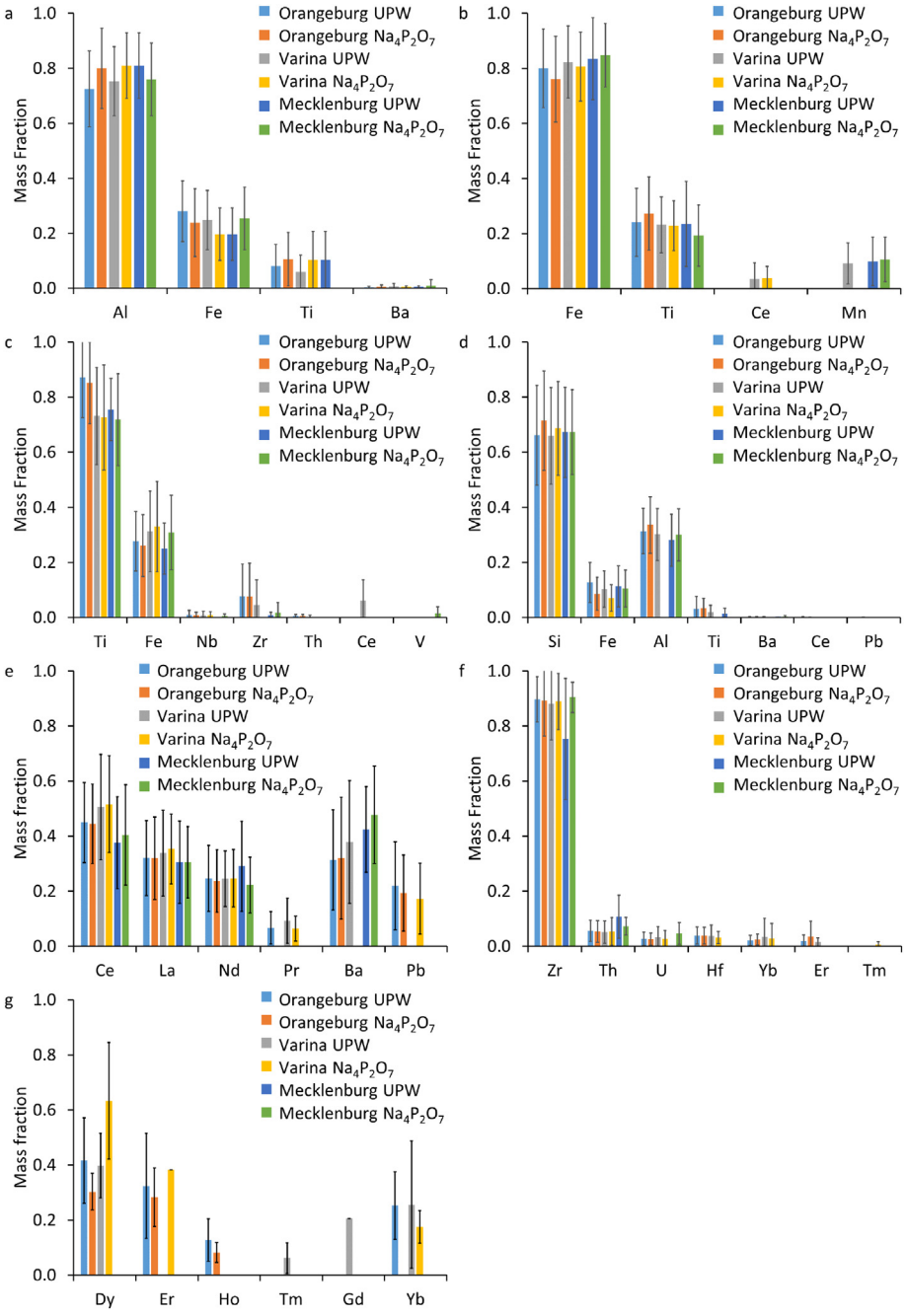

Fig. 4. Mean mass fraction of metals in different multi-metal nanomaterial clusters (a) AlFeTi, (b) FeTi, (C) TiFe, (d) SiFeAl, (e) CeLaNd, (f) ZrThU, and (g) DyErYb cluster. All data points are presented as mean ± standard deviation of the mass fraction of a given element in individual particles that occur in >10% of all NNMs within a given cluster.

$Na_4P_2O_7$-extracted suspensions than in UPW-extracted suspensions due to the increased disaggregation of Ti- and Fe-containing NNM heteroaggregates or dissolution of Fe in Ti- and Fe-containing particles (Regelink et al., 2013).

Two dominantly REE containing clusters were identified in most samples, representative of LREEs and HREEs (Fig. 3 and 4e and g). The LREE cluster contained dominantly Ce, La, Nd, Pr, Ba, Pb, and Th, whereas the HREE cluster contained Dy, Er, Ho, Tm, Gd, Tb, Th, and U (Fig. 4e and g). Additionally, REEs occurred in other clusters as trace elements including Si-, Al-, Fe-, Ti-, Zr-, and Mn-rich particle clusters. These observations are consistent with REE geochemistry. REE-bearing minerals generally contain most of the REE in varying concentrations but are usually dominated by either LREEs or HREEs (Haque et al., 2014; Walters et al., 2011). Thorium, as well as uranium, appear as components in many of these minerals (Haque et al., 2014; Ragheb, 2011). Minerals containing predominantly LREEs include bastnasite, monazite, allanite, loparite, ancylite, parasite, lanthanite, cheinite, cerite, stillwellite, britholite, fluocerite, and cerianite (Haque et al., 2014). Minerals containing predominantly HREEs include gadolinite, xenotime, samarskite, euxenite, fergusonite, yttrotantalite, yttrotungstite, and yttrialite. In addition to REE species, numerous other minerals may exhibit enrichment in REEs depending on their crystallization conditions; a few notable examples include titanite ($CaTiSiO_4O$), zircon ($ZrSiO_4$), eudialyte (Na—Ca—Mn—Fe—Zr cyclosilicate), pyrochlore $[Ca,Na)_{2-x}(NbTi)_2O_6(F,OH)]$, and members of the carnallite group $[(Ca,Sr,Ba,Pb)(Al,Fe)_3(PO_4)_2(OH)_5]$ (Chakhmouradian and Wall, 2012). The mineral apatite is generally enriched in the LREEs and the mineral zircon is generally enriched in the HREEs (Fig. 4f) (Aide and Aide, 2012).

It is also worth noting that predominantly impure metals occurred as minor elements in other phases. For instance, Nb occurred as a

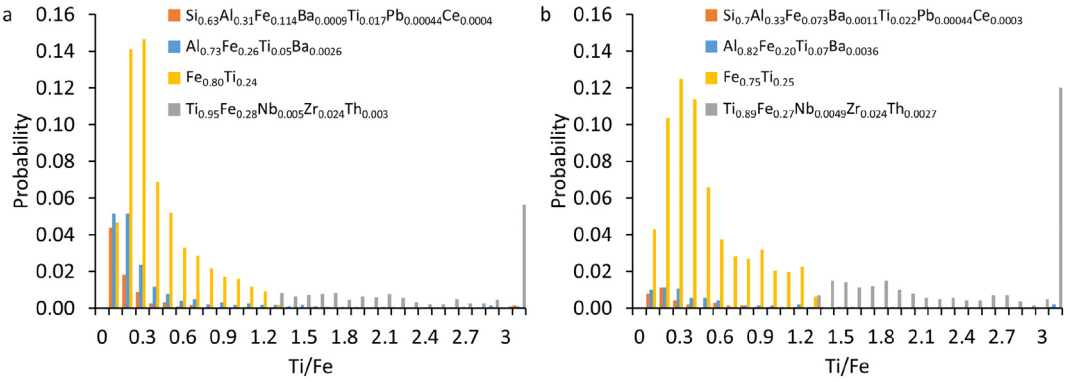

Fig. 5. Elemental ratio of Ti/Fe in Ti-containing clusters illustrated for Orangeburg soil (a) UPW-extracted suspensions, and (b) $Na_4P_2O_7$-extracted suspensions. The data was normalized to the total number of Ti and Fe containing particles. The cluster composition is derived from the mean mass fraction of each element in the cluster that occur in >10% of all NNMs within a given cluster.

trace metal in Ti-, Al-, Fe-, and Si-rich multi-metal clusters and was always associated with Ti in these clusters. Pb was detected as a minor element in Al-, Si-, Fe-, Ti-, Ce-, Mn-, and Ba-rich multi-metal clusters.

4. Conclusions

With the advancement of single particle analysis and the development of multi-element analysis within a single particle using SP-ICP-TOF-MS, there is an increased interest in differentiating ENMs from NNMs on a single particle basis in order to quantify the number and mass concentrations of ENMs in environmental systems. However, such analysis requires knowledge of the elemental composition of NNMs. Here we evaluated the impact of extractant composition (*e.g.*, UPW *vs.* $Na_4P_2O_7$ at pH 10) on the number concentration and composition of the extracted NM suspensions. In general, a higher number of total, single metal, and multi-metal NMs were detected for most elements in UPW-extracted suspensions than in $Na_4P_2O_7$-extracted suspensions. However, the elemental composition of the extracted multi-metal NNMs remained the same for both extractants with small shifts toward higher elemental ratios for Ti/Fe and Ti/Al in $Na_4P_2O_7$-extracted NNMs than in UPW-extracted NNMs. Here we identified NNMs that occur dominantly as single metal particles in natural soils (*e.g.*, Ti, Fe, Sn, Sb, and Tm); those that occur predominantly as multi metal NNMs (*e.g.*, V, Nb, Pr, Nd, Sm, Eu, Gd, Tb, Er, Dy, Yb, Lu, Hf, Ta, Pb, Th, and U); and those that occur as a mixture of single metal and multi metal NNMs (*e.g.*, Al, Si, Cr, Mn, Ni, Cu, Zn, Ba, La, Ce, W, and Bi). Consequently, it is possible to differentiate NNMs from ENMs based on particle purity only for those metals that occur predominantly as impure metals in NNMs. For other elements, other features are necessary in order to differentiate ENMs from NNMs. We also identified and determined the mean elemental composition of NNM clusters that accounted for the large majority of the detected multi-metal NNMs including Al-, Fe-, Ti-, Si-, Ce-, Zr-, and Dy-rich particles' cluster. Other sporadic NNM clusters were also identified in the investigated soils. The same trend in single and multi-metal particle abundances and the same major NNM clusters identified with the same elemental compositions were also identified in surface water samples (data not presented here). These findings serve as baseline information for the differentiation of ENMs from NNMs in environmental systems.

CRediT authorship contribution statement

Mohammed Baalousha: Conceptualization, Methodology, Writing – original draft, Writing – review & editing. **Jingjing Wang:** Investigation, Formal analysis, Writing – original draft, Writing – review & editing. **Mahdi Erfani:** Software, Writing – original draft, Writing – review & editing. **Erfan Goharian:** Software, Writing – original draft, Writing – review & editing.

Declaration of competing interest

The authors declare that they have no known competing financial interests or personal relationships that could have appeared to influence the work reported in this paper.

Acknowledgment

This work was supported by US National Science Foundation CAREER (1553909) grant and the MRI grant (1828055) to Dr. Mohammed Baalousha.

Appendix A. Supplementary data

Supplementary data to this article can be found online at https://doi.org/10.1016/j.scitotenv.2021.148426.

References

Aide, M.T., Aide, C., 2012. Rare earth elements: their importance in understanding soil genesis. Int. Schol. Res. Not. 2012.
Alvarez, P.J.J., Colvin, V., Lead, J., Stone, V., 2009. Research priorities to advance eco-responsible nanotechnology. ACS Nano 3 (7), 1616–1619.
Anthony, J.W., 1990. Handbook of Mineralogy: Halides, Hydroxides, Oxides. Vol. 3. Mineral Data Pub.
Baalousha, M., Wang, J., Nabi, M.M., Loosli, F., Valenca, R., Mohanty, S.K., Afrooz, N., Cantando, E., Aich, N., 2020. Stormwater green infrastructures retain high concentrations of TiO_2 engineered (nano)-particles. J. Hazard. Mater. 392, 122335.
Chakhmouradian, A.R., Wall, F., 2012. Rare earth elements: minerals, mines, magnets (and more). Elements 8 (5), 333–340.
Craigie, N., 2018. Principles of elemental chemostratigraphy. Advances in Oil and Gas Exploration & Production, Rudy Swennen. A Practical User Guide, p. 189 https://doi.org/10.1007/978-3-319-71216-1.
Durin, B., 2006. Transfert et transport colloïdal de polluants métalliques. Université de Nantes, Nantes, p. 376.
Fitzpatrick, R.W., Chittleborough, D., 2002. Titanium and zirconium minerals. Soil Miner. Environ. Appl. 7, 667–690.
Gaspar, J.C., Wyllie, P.J., 1983. Ilmenite (high Mg, Mn, Nb) in the carbonatites from the Jacupiranga complex, Brazil. Am. Mineral. 68 (9–10), 960–971.
Gondikas, A., von der Kammer, F., Kaegi, R., Borovinskaya, O., Neubauer, E., Navratilova, J., Praetorius, A., Cornelis, G., Hofmann, T., 2018. Where is the nano? Analytical approaches for the detection and quantification of TiO_2 engineered nanoparticles in surface waters. Environ. Sci. Nano 5 (2), 313–326.
Gondikas, A.P., von der Kammer, F., Reed, R.B., Wagner, S., Ranville, J.F., Hofmann, T., 2014. Release of TiO_2 nanoparticles from sunscreens into surface waters: a one-year survey at the Old Danube recreational lake. Environ. Sci. Technol. 48 (10), 5415–5422.
Gottschalk, F., Kost, E., Nowack, B., 2013. Engineered nanomaterials in water and soils: a risk quantification based on probabilistic exposure and effect modeling. Environ. Toxicol. Chem. 32 (6), 1278–1287.
Hadioui, M., Knapp, G.v., Azimzada, A., Jreije, I., Frechette-Viens, L., Wilkinson, K.J., 2019. Lowering the size detection limits of Ag and TiO_2 nanoparticles by single particle ICP-MS. Anal. Chem. 91 (20), 13275–13284.
Haque, N., Hughes, A., Lim, S., Vernon, C., 2014. Rare earth elements: overview of mining, mineralogy, uses, sustainability and environmental impact. Resources 3 (4), 614–635.
Hendriks, L., Gundlach-Graham, A., Hattendorf, B., Günther, D., 2017. Characterization of a new ICP-TOFMS instrument with continuous and discrete introduction of solutions. J. Anal. At. Spectrom. 32 (3), 548–561.

International Agency for Research on Cancer, 2010. Carbon Black, Titanium Dioxide, and Talc. Vol. 93. IARC Press.
Kaegi, R., Ulrich, A., Sinnet, B., Vonbank, R., Wichser, A., Zuleeg, S., Simmler, H., Brunner, S., Vonmont, H., Burkhardt, M., Boller, M., 2008. Synthetic TiO_2 nanoparticle emission from exterior facades into the aquatic environment. Environ. Pollut. 156 (2), 233–239.
Kaegi, R., Englert, A., Gondikas, A., Sinnet, B., von der Kammer, F., Burkhardt, M., 2017. Release of TiO_2-(nano) particles from construction and demolition landfills. NanoImpact 8, 73–79.
von der Kammer, F., Ferguson, P.L., Holden, P.A., Masion, A., Rogers, K.R., Klaine, S.J., Koelmans, A.A., Horne, N., Unrine, J.M., 2012. Analysis of engineered nanomaterials in complex matrices (environment and biota): general considerations and conceptual case studies. Environ. Toxicol. Chem. 31 (1), 32–49.
Lead, J.R., Batley, G.E., Alvarez, P.J., Croteau, M.N., Handy, R.D., McLaughlin, M.J., Judy, J.D., Schirmer, K., 2018. Nanomaterials in the environment: behavior, fate, bioavailability, and effects—an updated review. Environ. Toxicol. Chem. 37 (8), 2029–2063.
Lee, S., Bi, X., Reed, R.B., Ranville, J.F., Herckes, P., Westerhoff, P., 2014. Nanoparticle size detection limits by single particle ICP-MS for 40 elements. Environ. Sci. Technol. 48 (17), 10291–10300.
Long, K.R., Van Gosen, B.S., Foley, N.K., Cordier, D., 2012. The principal rare earth elements deposits of the United States: a summary of domestic deposits and a global perspective. Non-renewable Resource Issues. Springer, pp. 131–155.
Loosli, F., Berti, D., Yi, Z., Baalousha, M., 2018. Toward a better extraction and stabilization of titanium dioxide engineered nanoparticles in model water. NanoImpact 11, 119–127.
Loosli, F., Wang, J., Rothenberg, S., Bizimis, M., Winkler, C., Borovinskaya, O., Flamigni, L., Baalousha, M., 2019a. Sewage spills are a major source of titanium dioxide engineered (nano)-particle release into the environment. Environ. Sci. Nano 6 (3), 763–777.
Loosli, F., Yi, Z., Wang, J., Baalousha, M., 2019b. Improved extraction efficiency of natural nanomaterials in soils to facilitate their characterization using a multimethod approach. Sci. Total Environ. 677, 34–46.
Loosli, F., Yi, Z., Wang, J., Baalousha, M., 2019c. Dispersion of natural nanomaterials in surface waters for better characterization of their physicochemical properties by AF4-ICP-MS-TEM. Sci. Total Environ. 682, 663–672.
Mehrabi, K., Kaegi, R., Günther, D., Gundlach-Graham, A., 2021. Emerging investigator series: automated single-nanoparticle quantification and classification: a holistic study of particles into and out of wastewater treatment plants in Switzerland. Environ. Sci. Nano 8, 1211–1225.
Montano, M.D., Badiei, H.R., Bazargan, S., Ranville, J.F., 2014. Improvements in the detection and characterization of engineered nanoparticles using spICP-MS with microsecond dwell times. Environ. Sci. Nano 1 (4), 338–346.
Morad, S., 1986. SEM study of authigenic rutile, anatase and brookite in Proterozoic sandstones from Sweden. Sediment. Geol. 46 (1–2), 77–89.
Morad, S., Adin Aldahan, A., 1986. Alteration of detrital Fe-Ti oxides in sedimentary rocks. Geol. Soc. Am. Bull. 97 (5), 567–578.
Mücke, A., Chaudhuri, J.B., 1991. The continuous alteration of ilmenite through pseudorutile to leucoxene. Ore Geol. Rev. 6 (1), 25–44.
Murata, K., Rose Jr., H., Carron, M., Glass, J., 1957. Systematic variation of rare-earth elements in cerium-earth minerals. Geochim. Cosmochim. Acta 11 (3), 141–161.
Nakashima, K., Imaoka, T., 1998. Niobian and zincian ilmenites in syenites from Cape Ashizuri, Southwest Japan. Mineral. Petrol. 63 (1), 1–17.
Pace, H.E., Rogers, N.J., Jarolimek, C., Coleman, V.A., Higgins, C.P., Ranville, J.F., 2011. Determining transport efficiency for the purpose of counting and sizing nanoparticles via single particle inductively coupled plasma mass spectrometry. Anal. Chem. 83 (24), 9361–9369.
Philippe, A., Campos, D.A., Guigner, J.-M., Buchmann, C., Diehl, D., Schaumann, G.E., 2018. Characterization of the natural colloidal TiO_2 background in soil. Separations 5 (4), 50.
Piccinno, F., Gottschalk, F., Seeger, S., Nowack, B., 2012. Industrial production quantities and uses of ten engineered nanomaterials in Europe and the world. J. Nanopart. Res. Vol. 14. Springer Netherlands, pp. 1–11
Praetorius, A., Gundlach-Graham, A., Goldberg, E., Fabienke, W., Navratilova, J., Gondikas, A., Kaegi, R., Günther, D., Hofmann, T., von der Kammer, F., 2017. Single-particle multi-element fingerprinting (spMEF) using inductively-coupled plasma time-of-flight mass spectrometry (ICP-TOFMS) to identify engineered nanoparticles against the elevated natural background in soils. Environ. Sci. Nano 4 (2), 307–314.
Ragheb, M., 2011. Thorium Resources in Rare Earth Elements. December.
Regelink, I.C., Weng, L., Koopmans, G.F., Van Riemsdijk, W.H., 2013. Asymmetric flow field-flow fractionation as a new approach to analyse iron-(hydr)oxide nanoparticles in soil extracts. Geoderma 202, 134–141.
Tang, Z., Wu, L., Luo, Y., Christie, P., 2009. Size fractionation and characterization of nanocolloidal particles in soils. Environ. Geochem. Health 31 (1), 1–10.
Tanner, M., 2010. Shorter signals for improved signal to noise ratio, the influence of Poisson distribution. J. Anal. At. Spectrom. 25 (3), 405–407.
Walters, A., Lusty, P., Hill, A., 2011. British Geological Survey: Rare Earth Elements. Natural Environment Research Council http://www.bgs.ac.uk/mineralsuk.
Wang, J., Nabi, M.M., Mohanty, S.K., Afrooz, A.N., Cantando, E., Aich, N., Baalousha, M., 2020. Detection and quantification of engineered particles in urban runoff. Chemosphere 248, 126070.
Weibel, R., 2003. Alteration of detrital Fe-Ti oxides in Miocene fluvial deposits, central Jutland, Denmark. Bull. Geol. Soc. Den. 50 (2), 141–208.
Yi, Z., Loosli, F., Wang, J., Berti, D., Baalousha, M., 2020. How to distinguish natural versus engineered nanomaterials: insights from the analysis of TiO_2 and CeO_2 in soils. Environ. Chem. Lett. 18 (1), 215–227.
Zack, T., Kronz, A., Foley, S.F., Rivers, T., 2002. Trace element abundances in rutiles from eclogites and associated garnet mica schists. Chem. Geol. 184 (1–2), 97–122.